Evaluation of Hybrid Broadband Ground Motion Simulations for Response History Analysis and Design

Lynne S. Burks,[a] M.EERI, **Reid B. Zimmerman,**[b] M.EERI, and **Jack W. Baker,**[a] M.EERI

Chapter 16 of ASCE 7 governs the selection of ground motions for analysis of new buildings and requires recordings that meet specified criteria. If a sufficient number of recordings cannot be found, it allows the use of "appropriate simulated ground motions," but does not provide further guidance. This paper outlines a procedure for generating and selecting a set of "appropriate" hybrid broadband simulations and a comparable set of recordings. Both ground motion sets are used to analyze a building in Berkeley, California, and the predicted structural performance is compared. The structural behavior resulting from recordings and simulations is similar, and most discrepancies are explained by differences in directional properties such as orientation of the maximum spectral response. These results suggest that when simulations meet the criteria outlined for recordings in ASCE 7 and properties such as directionality are realistically represented, simulations provide useful results for structural analysis and design. [DOI: 10.1193/091113EQS248M]

INTRODUCTION

Engineers typically use earthquake ground motion records as input for nonlinear response history analysis of structural models. Ground motion selection for this type of analysis is governed in the building code by Chapter 16 of ASCE 7 (ASCE 2010). Significant updates to this chapter are currently under consideration, but the basic process of ground motion selection will remain similar (Haselton et al. 2014). Ground motion records are selected to match a target spectrum that is based on the maximum considered earthquake (MCE_R) determined from seismic hazard analysis. Selected recordings are then scaled such that the "average value for the 5% damped response spectra for the suite of ground motions is not less than the design response spectrum" and they must come from an earthquake "consistent with those that control the MCE_R" (ASCE 2010). If enough appropriate recordings do not exist, then use of "appropriate simulated ground motions" is allowed. But there is no definition of what makes a ground motion simulation "appropriate" and no guidance on what type of simulations to use.

There are many methods of ground motion simulation, including stochastic-process-based simulations (e.g., Der Kiureghian and Crempien 1989, Jurkevics and Ulrych 1978,

---

[a] Civil & Environmental Engineering Department, Stanford University, Stanford, CA 94305
[b] Rutherford + Chekene, San Francisco, CA 94105

Mobarakeh et al. 2002, Pousse et al. 2006, Rezaeian and Der Kiureghian 2010), stochastic point source and finite fault (e.g., Beresnev and Atkinson 1997, Boore 1983, Hanks and McGuire 1981, Motazedian and Atkinson 2005), and hybrid broadband (e.g., Graves and Pitarka 2010; Hartzell et al. 2005, 1999; Mai et al. 2010; Schmedes et al. 2010). Hybrid broadband simulations are typically considered "state of the art" for structural analysis applications because they use a combination of deterministic and stochastic techniques to simulate ground motion time histories across a wide frequency range and in three components of motion. The long period portion of the time history (typically greater than 1 s) is computed using deterministic methods that account for the fault rupture and wave propagation paths. At short periods (typically less than 1 s), deterministic methods are not yet practical to implement due to incomplete knowledge of source radiation and wave propagation at high frequencies and imprecisely known Earth structure at short scale lengths. Therefore, the short period portion is typically computed using stochastic methods and then splice to the long period portion.

Regardless of the simulation approach, the resulting ground motions must be validated to ensure that they produce structural demands similar to those of real motions in order to be used with confidence in engineering applications. The majority of past validation efforts have focused on select scenario earthquakes and the accuracy of ground motion amplitude, such as shaking intensity or spectral acceleration at a few periods (e.g., Aagaard et al. 2008; Frankel 2009; Hartzell et al. 2005, 1999; Star et al. 2011). This type of validation is crucial for using simulations in seismic hazard analysis, but does not represent the way a structural engineer will use ground motion simulations in the analysis and design of a building. There has been some study on the structural response to simulated ground motions (e.g., Galasso et al. 2013, 2012, Iervolino et al. 2010, Jayaram and Shome 2012, Jones and Zareian 2013), but little focus has been placed on the building code with respect to ground motion selection and acceptance criteria. In building code applications, engineers first compute a target spectrum using seismic hazard analysis and then select ground motions with elastic response spectra that match the target. This process presents two opportunities for the use of ground motion simulations: (1) in seismic hazard analysis to determine the target spectrum, where most validation efforts are currently focused, and (2) in structural analysis to determine demands produced by a suite of ground motions that match the target spectrum. This paper focuses on validation of the s use of ground motion simulations in the context of the proposed update to ASCE 7 guidelines (Haselton et al. 2014).

We analyze a three-dimensional (3-D) nonlinear model of a real building using a set of recordings and a comparable set of hybrid broadband simulations, selected according to the proposed ASCE 7 procedure. First, we compute the target spectrum for the building and selected appropriate ground motion recordings. Then we generate and select appropriate hybrid broadband ground motion simulations. Finally, we evaluate the structure's performance and find that seismic demands are similar for the suites of recordings and simulations.

BUILDING OVERVIEW

The structural model used for this study is based on an actual building designed by Rutherford + Chekene and located 1 km from the Hayward Fault in Berkeley, California (Figure 1; Zimmerman et al. 2014). The near-fault location of this site makes the use of
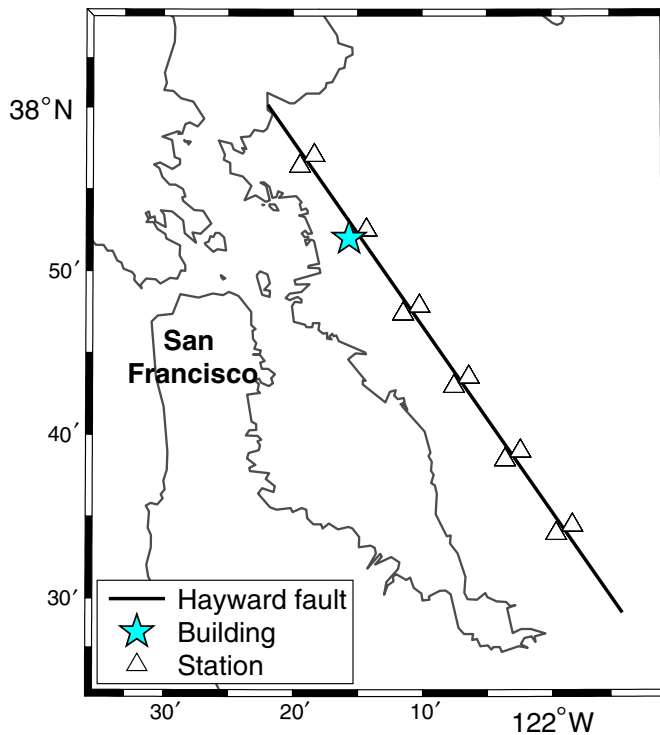
Figure 1. Map of the Hayward fault, building considered in this study, and 11 other stations at which ground motions were simulated (discussed in ground motion simulations section), each at a distance of 1 km from the fault.

simulations appealing because it is difficult to find a sufficient number of representative near-fault recordings. The building's lateral force resisting system consists of steel special moment resisting frames (SMRF) in the fault-normal direction and buckling-restrained braced frames (BRBF) in the fault-parallel direction (Figure 2). The building has five stories (84 ft) above grade and one story (18 ft) below grade consisting of reinforced concrete perimeter walls. The first and s mode periods for the SMRF are 1.67 s and 0.57 s, respectively, and for the BRBF are 1.08 s and 0.35 s (Figure 3). The site is located on soil with an average shear wave velocity in the top 30 m (V_{S30}) of 500 m/s (Rutherford + Chekene 2002).

GROUND MOTION SELECTION

The seismic design of structures is based on a target spectrum defined by the building code. Engineers use response history analysis for designing new buildings (particularly isolated or non-conforming systems), evaluating existing buildings for retrofit, or performing performance-based assessments. These procedures require ground motion records as input rather than just a target spectrum. This section outlines the computation of the target spectrum and the selection of consistent ground motion recordings and simulations following the proposed ASCE 7 procedure. Some key relevant differences between Chapter 16 of ASCE 7-10
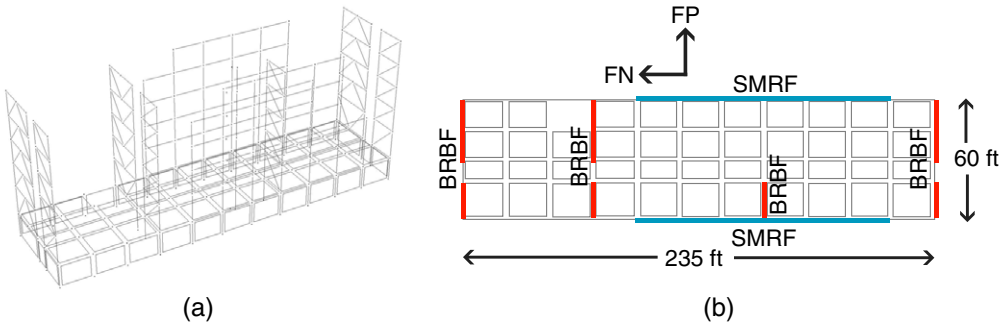
Figure 2. (a) Three-dimensional view and (b) floor plan view of the structural model with steel special moment resisting frames (SMRF) in the fault-normal direction and buckling-restrained brace frames (BRBF) in the fault-parallel direction.
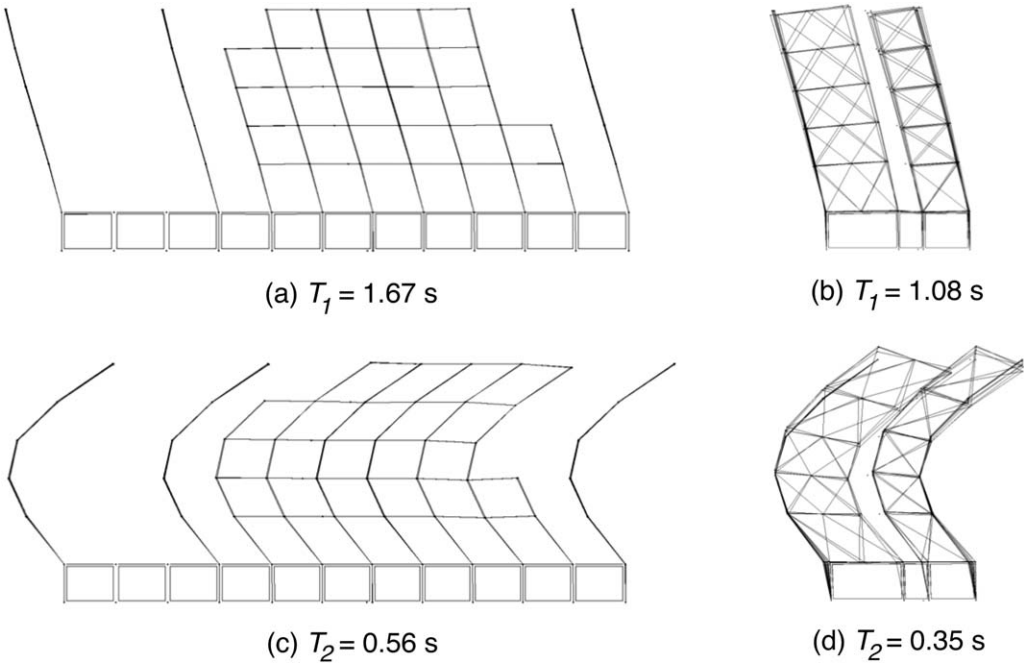

(a) $T_1 = 1.67$ s

(b) $T_1 = 1.08$ s

(c) $T_2 = 0.56$ s

(d) $T_2 = 0.35$ s

Figure 3. First two modes of vibration for each direction of the structural model: (a) first mode of SMRF with $T = 1.67$ s, (b) first mode of BRBF with $T = 1.08$ s, (c) s mode of SMRF with $T = 0.56$ s, and (d) s mode of BRBF with $T = 0.35$ s.

and the proposed procedure are the use of the maximum considered earthquake (MCE$_R$) rather than design basis earthquake (DBE) spectrum for analysis, the use of an $Sa_{RotD100}$ (discussed in the next section) rather than a geometric mean target spectrum, and an increase to 11 required ground motions for response history analysis (Haselton et al. 2014).

TARGET SPECTRUM

A site-specific MCE_R spectrum was computed using USGS site-specific hazard curves, following the procedure of the proposed ASCE 7 Chapter 21 (Zimmerman et al. 2014). This MCE_R spectrum, which represents a geometric mean spectrum, was then modified by the NEHRP "maximum direction factors" (BSSC, 2009) to represent an $Sa_{RotD100}$ spectrum (shown in Figure 4), which is the maximum spectral acceleration in any orientation. For a multi-component ground motion, a spectral acceleration value can be computed for the shaking in any horizontal direction. For a given period, spectral accelerations are computed for rotation angles from 0° to 180° (because 180° to 360° are redundant), and Sa_{RotDnn} is the nnth percentile of the results. Thus $Sa_{RotD100}$ is the maximum and Sa_{RotD50} is the median of the spectral accelerations over all unique horizontal directions (Boore, 2010, Boore et al. 2006). The site-specific $Sa_{RotD100}$ spectrum was then compared to the design response spectrum of ASCE 7 section 11.4.5, and since the site-specific spectrum was less than 80% of the design response spectrum, ASCE 7 required that the resulting target spectrum was essentially 80% of the design response spectrum (Zimmerman et al. 2014).

The shape of the target spectrum is given by the building code and therefore cannot be influenced by ground motion simulations. Furthermore, it is not the role of the engineer to change the target spectrum for a given project. The goal of this study is not to assess the adequacy of the target spectrum or building code procedure, but rather to test how well simulations fit into the existing procedure.
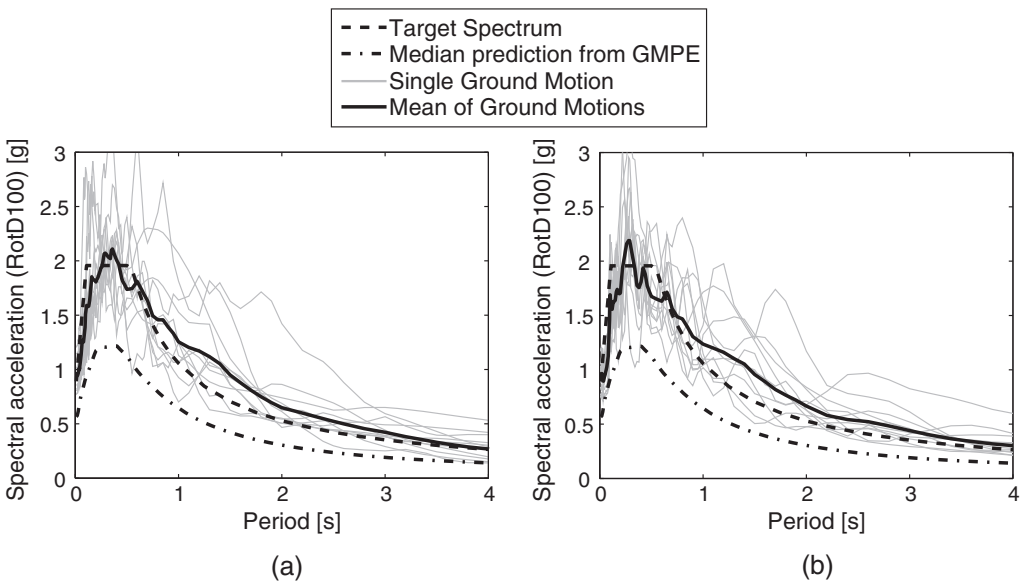

Figure 4. $Sa_{RotD100}$ spectra for the chosen 11 ground motion (a) recordings and (b) hybrid broadband simulations, shown in comparison to the target spectrum and the median prediction from a ground motion prediction equation (GMPE).

GROUND MOTION RECORDINGS

Eleven recorded time histories were selected from the Pacific Earthquake Engineering Center's (PEER) Next Generation Attenuation (NGA) ground motion database (Chiou et al. 2008) based on their $Sa_{RotD100}$ spectra, after first screening by magnitude, distance, V_{S30}, and near-fault characteristics. Seismic hazard deaggregation for the building site produces a modal MCE_R earthquake of magnitude 6.98 on the nearby Hayward fault (USGS, 2008). Therefore recordings from earthquakes with magnitudes between 6.4 and 7.6 and with closest distances to the fault rupture between 0 km and 15 km were considered for selection. Site conditions were allowed to differ by up to one class relative to the actual site, resulting in records with V_{S30} values from 202 m/s to 629 m/s. Because the building is at a near-fault site, the recordings were selected to have strong velocity pulses with pulse periods from 1.2 s to 12.9 s, consistent with the target causal earthquakes' magnitudes (Bray and Rodriguez-Marek 2004, Shahi and Baker 2011). All recordings came from active crustal regions, with no restrictions placed on the rupture mechanism.

After filtering by magnitude, distance, V_{S30}, and pulse characteristics, the remaining candidate ground motion recordings were scaled uniformly to best match the target spectrum between 0.2 s and 3.36 s. A maximum scale factor of 4 was imposed and no more than 3 recordings from any single event were allowed. Ground motions were selected by first computing the sum of square error between the log of the target spectrum and the log of each scaled recorded spectrum over the period range of interest, and then choosing the 11 ground motions with the smallest error, subject to the above restrictions. Table 1 lists the 11 selected recordings, Figure 4a shows their $Sa_{RotD100}$ spectra, and Figure 5 shows some sample velocity time histories.

Table 1. The 11 selected ground motion recordings

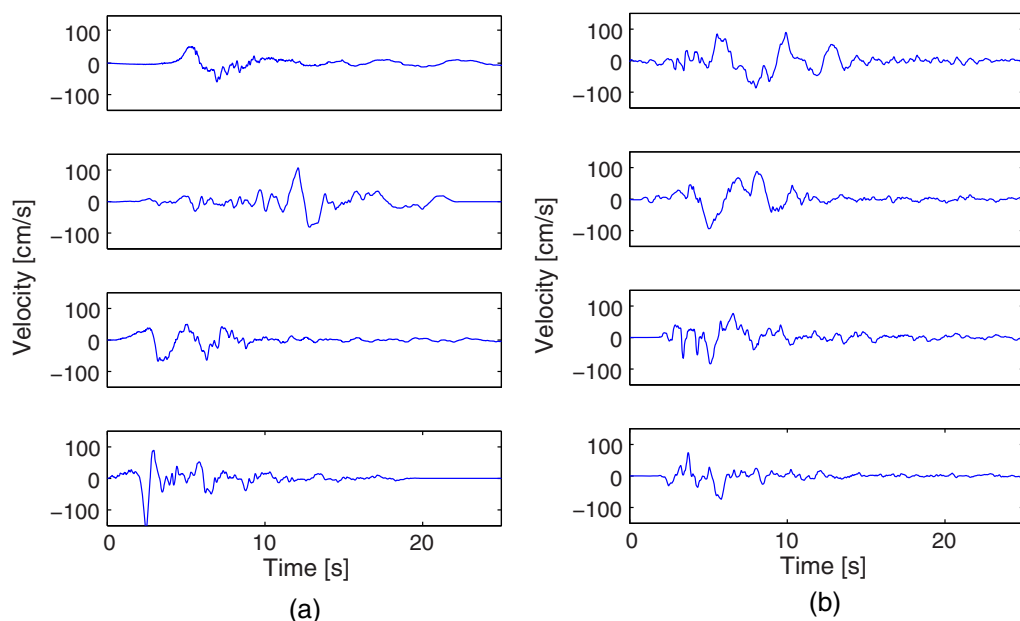| NGA #	Earthquake	Station	Magnitude	Distance (km)	V_{S30} (m/s)	Scale factor	Pulse period (s)
179	Imperial Valley-06	El Centro Array #4	6.5	7.1	209	1.9	4.6
183	Imperial Valley-06	El Centro Array #8	6.5	3.9	206	1.9	5.4
184	Imperial Valley-06	El Centro Differential Array	6.5	5.1	202	1.7	5.9
723	Superstition Hills-02	Parachute Test Site	6.5	1.0	349	1.7	2.3
802	Loma Prieta	Saratoga – Aloha Ave.	6.9	8.5	371	2.2	4.5
983	Northridge-01	Jensen Filter Plant Generator	6.7	5.4	526	0.9	3.5
1013	Northridge-01	LA Dam	6.7	5.9	629	1.9	1.7
1063	Northridge-01	Rinaldi Receiving Station	6.7	6.5	282	1.0	1.2
1202	Chi-Chi, Taiwan	CHY035	7.6	12.7	474	2.6	1.4
1493	Chi-Chi Taiwan	TCU053	7.6	6.0	455	3.6	12.9
1528	Chi-Chi Taiwan	TCU101	7.6	2.1	273	2.9	10.0

Figure 5 Sample velocity time histories from the selected (a) recordings and (b) simulations.

GROUND MOTION SIMULATIONS

SOUTHERN CALIFORNIA EARTHQUAKE CENTER (SCEC) BROADBAND PLATFORM

The Southern California Earthquake Center's (SCEC) Broadband Platform is a software system that makes hybrid broadband simulation codes available to outside users (SCEC 2012). A number of scientific researchers have contributed modules to the Broadband Platform for rupture generation, low frequency seismogram synthesis, high frequency seismogram synthesis, and nonlinear site effects (Graves and Pitarka 2010, Mai et al. 2010, Motazedian and Atkinson 2005, Schmedes et al. 2010, Zeng et al. 1994). In order to simulate ground motions on the Broadband Platform, the user provides a simple description of the rupture including magnitude, hypocenter location, rupture dimensions, and dip, strike, and rake for a single-plane fault surface. The rupture generator module takes this information and generates a detailed time history of slip on the rupture surface. The user also provides a list of the latitude, longitude, and V_{S30} of stations at which to simulate ground motion time histories. The low frequency synthesis module deterministically computes a low frequency seismogram, and the high frequency synthesis module stochastically generates a high-frequency seismogram, and they are then spliced together at a frequency of about 1 Hz. Once the broadband seismogram is generated, an empirical site amplification is applied to its Fourier spectrum based on the site's target V_{S30} value. The final result is an acceleration time history at each specified station with three components of motion (i.e., north-south, east-west, and vertical). The Broadband Platform, which is intended for widespread use of well-understood
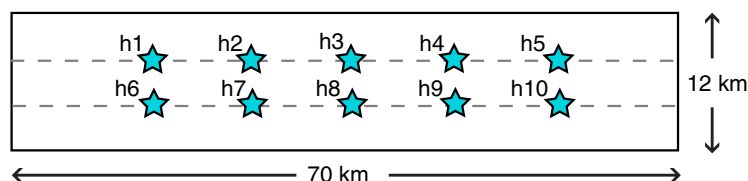
Figure 6. Cross section of the simulated rupture surface based on the Hayward fault, with 10 hypocenter locations shown as stars and labeled as *h1* to *h10*.

algorithms, is currently limited to planar faults and one-dimensional (1-D) Green's functions, but alternative implementations of these hybrid broadband algorithms outside the platform overcome those limitations (e.g., Aagaard et al. 2010, 2008).

EARTHQUAKE SCENARIO

The seismic hazard deaggregation for the building site produces a modal earthquake of magnitude 6.98 at a distance of 2.1 km (USGS 2008), so a scenario earthquake was chosen for the simulations to be a magnitude 7 vertical strike-slip earthquake on the Hayward fault. The Hayward fault has a strike of 322°, a history of surface rupture (i.e., depth of 0 km), and a length of 70 km and width of 12 km were chosen to be consistent with the rupture area of a magnitude 7 earthquake (Wells and Coppersmith 1994). Ten ruptures were simulated on this fault, each with a unique hypocenter location (Figure 6). Twelve stations were defined around the fault, including the actual building location and 11 other sites, each also at a distance of 1 km and with $V_{S30} = 500 \, \mathrm{m/s}$ (Figure 1). In principle, simulations could have been produced for only the exact location of interest, but this approach was used to efficiently obtain a greater number of time histories because simulating each rupture is the most computationally expensive step of the process, and it was anticipated that simulations at the additional stations would be representative of those at the actual building location.

GENERATION AND SELECTION OF GROUND MOTION SIMULATIONS

Using version 11.2.3 of the Broadband Platform, we simulated 10 ruptures at 12 stations using the Graves and Pitarka (2010; GP) method for all scientific modules including the rupture generator, low frequency, high frequency, and nonlinear site response (hereafter referred to as "GP simulations"). The $Sa_{RotD100}$ spectra of the simulations tend to be much larger at long periods than the corresponding median prediction from an empirical ground motion prediction equation (GMPE, previously known as attenuation relationship; Figure 7a). This amplification is partially due to approximations resulting from the Broadband Platform's use of Green's functions computed for a layered 1-D model and to strong directivity effects from a single planar strike-slip fault that is surface-rupturing, though it might also be partially due to under-prediction of ground motions by empirical GMPEs in this case that is not well constrained by recordings (Graves and Olsen 2013, *pers. comm.*). The $Sa_{RotD100}$ spectra better match the median GMPE prediction at short periods because this portion of the seismogram is stochastically generated based on the expected level of shaking. The resulting spectra generally have a large dip near 1 s, where high
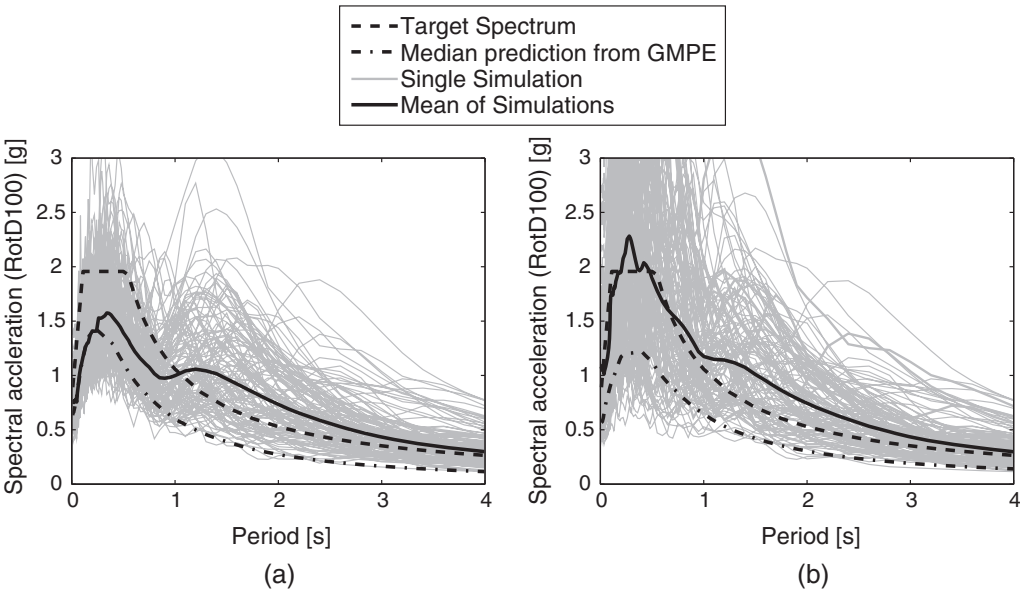
Figure 7. $Sa_{RotD100}$ spectra of all 120 (a) GP simulations and (b) SDSU simulations.

and low frequency seismograms are spliced together using matched Butterworth filters (Graves and Pitarka 2010). The difference in amplitude may be due to the stress drop used in the high frequency module, which is hard-coded into the broadband platform. The unusual shape of these spectra makes it difficult to match any of these simulations to the target spectrum.

We repeated the simulations using the Mai et al. (2010) (SDSU, i.e., BBtoolbox version 1.4) method for high frequency and nonlinear site response and the GP method for rupture generator and low frequency (hereafter referred to as "SDSU simulations"). The spectra of these simulations are more consistent with the target spectrum (Figure 7b) because the SDSU method scales the high frequency portion of the seismogram to match the low frequency portion. For this reason, we selected ground motions from the SDSU simulations for this study. Some sample velocity time histories are shown in Figure 5.

From the set of 120 SDSU ground motion simulations, 11 simulations were selected (Figure 4b and Figure 5). To ensure that any potential differences in the structural analysis results were due to differences in the time series rather than response spectra, simulations were selected based on the similarity of their $Sa_{RotD100}$ spectra to the 11 chosen recordings. The sum of squared difference was computed between each recording's $Sa_{RotD100}$ spectrum and the $Sa_{RotD100}$ spectrum of each simulation, and then the simulation with the smallest difference was selected. The resulting set of simulations has a mean spectral shape that is nearly identical to the mean spectral shape of the recordings. Another ground motion selection approach would be to independently select recordings and simulations to match the target spectrum and identify potential discrepancies, such as variability, but that method was not explored further here.

It is notable that from a seismic hazard analysis perspective, these simulations would likely not be helpful because their response spectra are much larger than corresponding empirical predictions and comparable recordings for this earthquake scenario, and the differences are at least in part due to limitations of the source modeling and simulation approach used here. Nonetheless, this does not exclude these simulations from a building code analysis because the ground motion spectrum in the building code is specified by an independent hazard analysis rather than by the "typical" spectra of the simulations. As long as simulations can be obtained with spectra and other properties appropriate for the situation of interest, they may be suitable for a code analysis, as will be explored further below.

DIRECTIONAL PROPERTIES OF THE GROUND MOTION SIMULATIONS

Though the chosen recordings and simulations have nearly identical $Sa_{RotD100}$ spectra, their fault-normal and fault-parallel component response spectra are different (Figure 8). The mean response spectrum of simulations is 10–15% larger than recordings in the fault-normal direction and 20–40% smaller in the fault-parallel direction at periods longer than 1 s. The ratio of the fault-normal to the fault-parallel spectra of the simulations is thus much larger than recordings at periods longer than 1 s (Figure 9), where the ratio of simulations is 1.5 times recordings at 2 s and 2.5 times recordings at 7 s. This amplified ratio indicates that the simulations excite an SDOF relatively more than the recordings in the fault-normal direction and are therefore more polarized.

Another directional property to consider for each ground motion is the ratio of $Sa_{RotD100}$ to Sa_{RotD50}, which indicates the polarization of SDOF response over all possible horizontal orientations. If the ratio is large, then the maximum response is much larger than the median, indicating that the oscillator response is polarized or amplified in a single direction. For all ground motion recordings in the PEER NGA database (regardless of magnitude, distance, and earthquake rupture mechanism) the $Sa_{RotD100}$ to Sa_{RotD50} ratio is very robust, so the
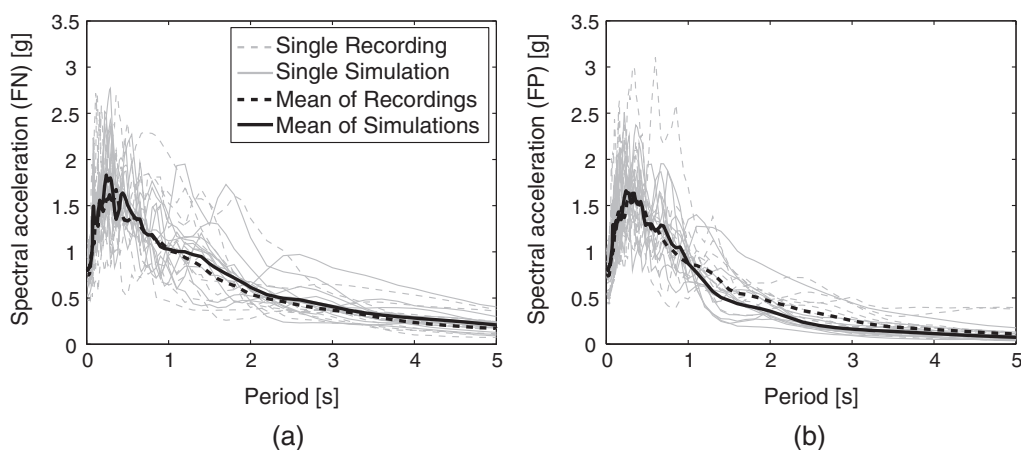

Figure 8. Response spectra for the chosen 11 ground motion recordings and simulations in the (a) fault-normal and (b) fault-parallel direction.
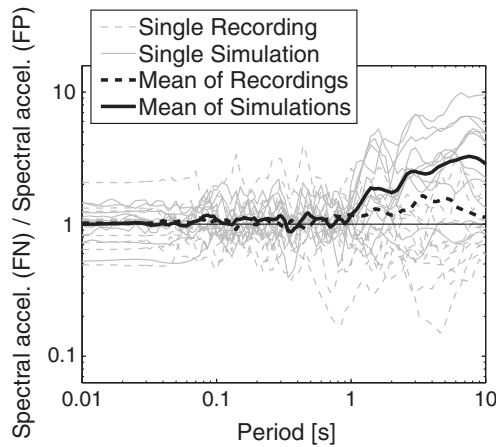
Figure 9. Ratio of the response spectra in the fault-normal direction to the fault-parallel direction for the chosen 11 ground motion recordings and simulations.

geometric mean $Sa_{RotD100}$ to Sa_{RotD50} ratio of all 120 GP and SDSU simulations and 11 recordings are compared to two empirical predictions (Figure 10; Beyer and Bommer 2006, Shahi and Baker 2013). The sample size of recordings is much smaller than simulations, but the difference between the geometric mean ratio of recordings and simulations at periods longer than 1 s is larger than the standard error of the mean of recordings (which ranges from 0.02 to 0.04). The GP and SDSU simulations are essentially identical at long periods because they were both computed using the GP method for low frequencies, and their $Sa_{RotD100}$ to Sa_{RotD50} ratios at long periods are larger than the empirical predictions, indicating
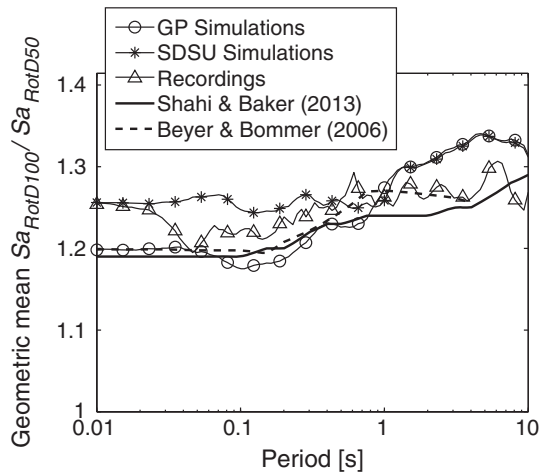

Figure 10. Geometric mean $Sa_{RotD100}/Sa_{RotD50}$ for all 120 GP and SDSU simulations and 11 recordings compared to empirical predictions.

that the simulations are more polarized than the recordings (see Burks and Baker 2014). This is probably due to exaggerated directivity effects in the simulations (as discussed in the previous section). For the SDSU simulations, the polarization at long periods is carried over to short periods because the high frequency seismogram is scaled.

The distribution of $Sa_{RotD100}$ to Sa_{RotD50} ratios for the SDSU simulations is compared to the set of recordings at select periods (Figure 11). At periods below 1 s, the distribution of ratios appears nearly uniform for both the simulations and recordings, as expected (Shahi and Baker 2013). But at $T = 1.2$ s, the ratio of the simulations starts to skew relative to recordings and becomes extremely skewed at $T = 5$ s.

To demonstrate the effect of the $Sa_{RotD100}$ to Sa_{RotD50} ratio on SDOF response, consider the displacement trace of several SDOF oscillators with varying period (Figure 12). The response to two ground motion simulations are shown for each SDOF: (1) a simulation with $Sa_{RotD100}/Sa_{RotD50} \approx 1$, which is the minimum possible ratio, and (2) a simulation with $Sa_{RotD100}/Sa_{RotD50} \approx 1.42$, which is the maximum possible ratio. For all periods, the SDOF response to the simulation with a ratio of 1 tends to be relatively uniform in all directions and the response to the simulation with a ratio of 1.42 tends to be strongly polarized in a single direction. Because most simulations have a large ratio at long periods (Figure 11d), engineers will observe more polarization in the response of long period structures to currently available hybrid broadband simulations than comparable recordings.
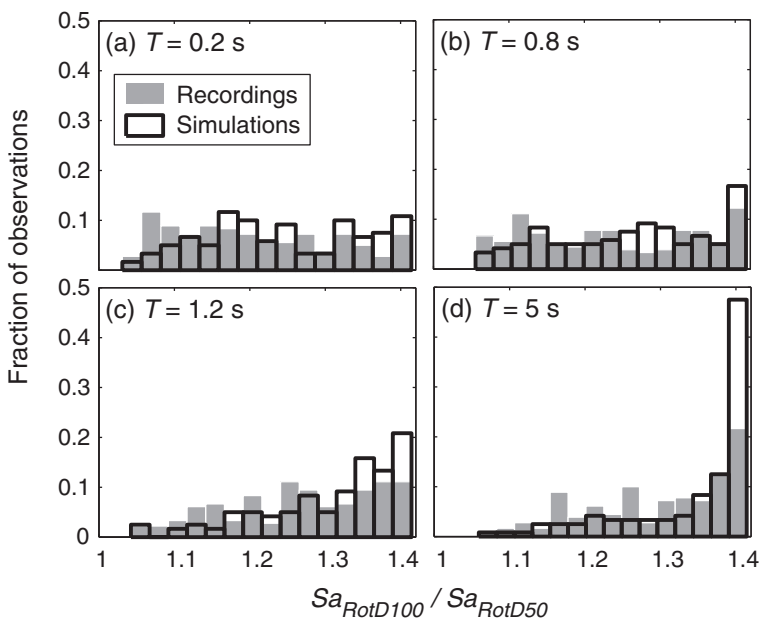

Figure 11 Histogram of the $Sa_{RotD100}$ to Sa_{RotD50} ratio for all SDSU simulations and a set of comparable recordings at (a) $T = 0.2$ s, (b) $T = 0.8$ s, (c) $T = 1.2$ s, and (d) $T = 5$ s.
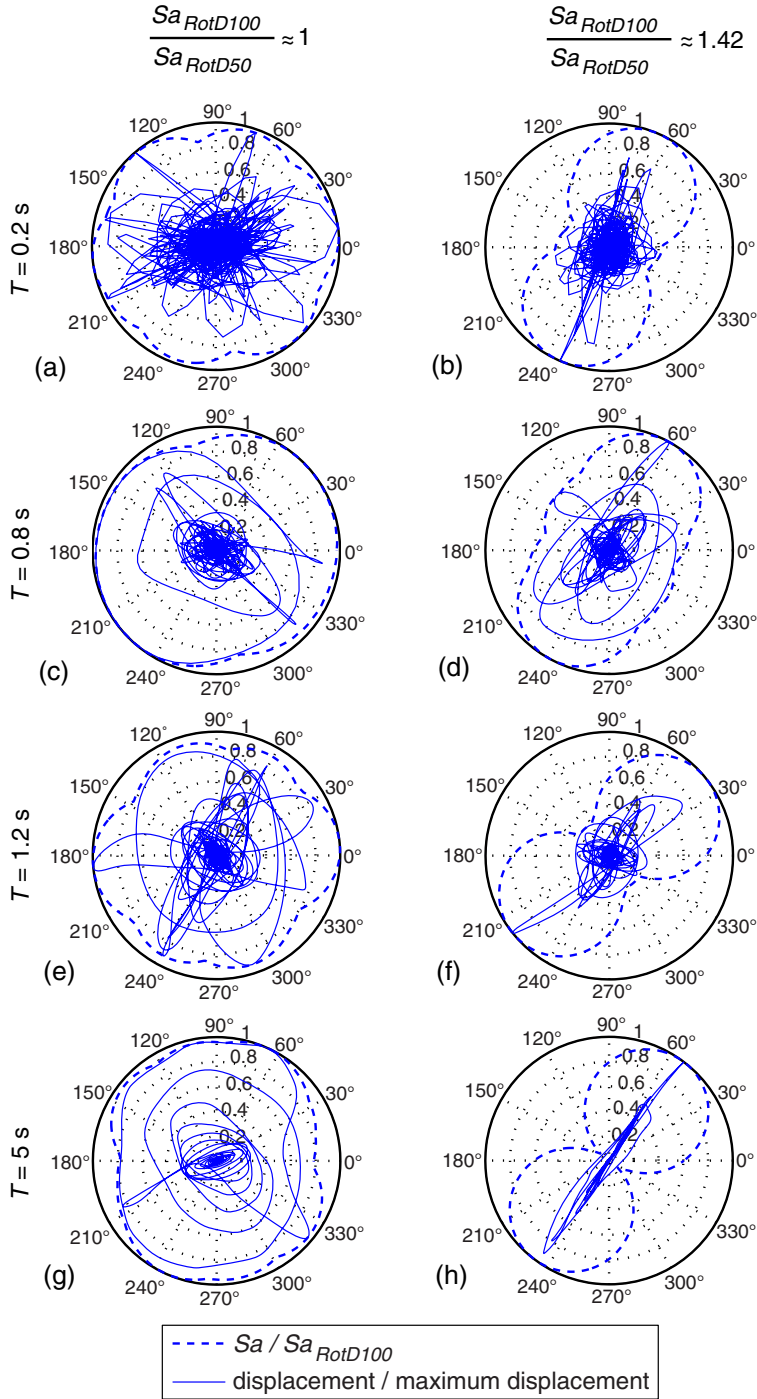
Figure 12. Displacement trace of the response of an SDOF oscillator to a ground motion simulation with (a) $T = 0.2\,\text{s}$ and $Sa_{RotD100}/Sa_{RotD50} \approx 1$, (b) $T = 0.2\,\text{s}$ and $Sa_{RotD100}/Sa_{RotD50} \approx 1.42$, (c) $T = 0.8\,\text{s}$ and $Sa_{RotD100}/Sa_{RotD50} \approx 1$, (d) $T = 0.8\,\text{s}$ and $Sa_{RotD100}/Sa_{RotD50} \approx 1.42$, (e) $T = 1.2\,\text{s}$ and $Sa_{RotD100}/Sa_{RotD50} \approx 1$, (f) $T = 1.2\,\text{s}$ and $Sa_{RotD100}/Sa_{RotD50} \approx 1.42$, (g) $T = 5\,\text{s}$ and $Sa_{RotD100}/Sa_{RotD50} \approx 1$, (h) $T = 5\,\text{s}$ and $Sa_{RotD100}/Sa_{RotD50} \approx 1.42$.

STRUCTURAL ANALYSIS AND RESULTS

The previously described building was modeled in three dimensions using PERFORM-3D software and nonlinear response history analysis was performed using the previously described sets of 11 ground motion recordings and simulations. The building model accounts for the building geometry, expected gravity loading, restraint conditions, P-Delta effects, viscous damping, and element stiffness and nonlinear behavior. Details on the modeling of elements and plastic hinges are provided in Zimmerman et al. (2014).

The mean drift demand on the structure is similar between the recordings and the simulations (Figure 13). For both ground motion sets, drifts are larger and more variable in the fault-normal direction than the fault-parallel because of the difference in lateral force-resisting system, that is, a moment frame versus a braced frame, respectively. Moment frames are generally more ductile than braced frames and tend to have a larger and more variable displacement response. However, the mean drift from simulations is up to 20% larger than the mean drift from recordings in the fault-normal direction and about 10% smaller in the fault-parallel direction. But these differences are not statistically significant using a t-test at a 5% level, due to the small number of ground motions used in this procedure. This discrepancy can be partially explained by the difference in elastic response spectra of the simulations and recordings in these orientations (Figure 8). Also, the drift from at least one recording and two simulations far exceeds the others, which slightly skews the mean drift.
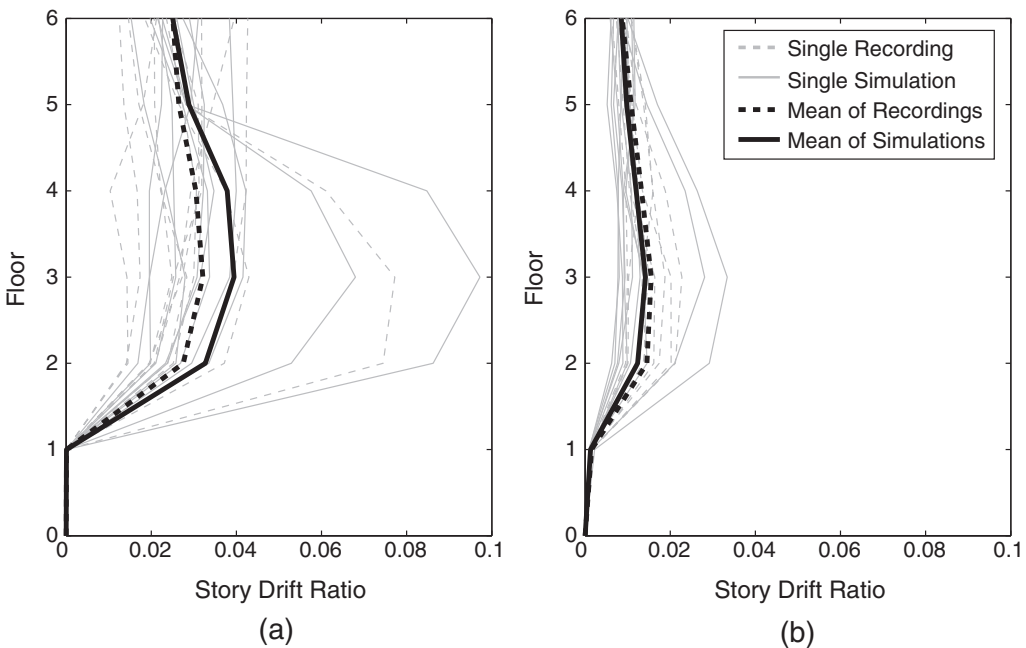

Figure 13. Drift demand from the set of recorded and simulated ground motions in the (a) fault-normal and (b) fault-parallel directions.

The story shear for the recordings and simulations is reported in Figure 14. In both directions, the variability in story shear is less than the variability in drift because a plastic mechanism forms due to nonlinear force-displacement behavior. If an individual ground motion causes this mechanism, the story shear can only increase modestly through means such as strain hardening, resulting in minimal changes to the final story shear. However, similar to the trend in drift, the increased polarization of the simulations produces mean story shears that are about 4% larger than recordings in the fault-normal direction and 8% smaller in the fault-parallel. But the motions that produce outliers in drift do not produce outliers in story shear and therefore the mean is less affected.

Plastic rotation and plastic strain demands were checked for local elements (Figure 15). For each element, the ratio of demand to limit indicates whether the computed level of demand is acceptable. The demand is defined as the mean over all ground motions in each set and the limit is defined as the point at which a structural member action can no longer carry gravity load times some factor less than one that varies depending on element type (Zimmerman et al. 2014). Although some elements are non-conforming, meaning their demand-to-limit ratio exceeds one, for both ground motion sets the general trends in element checks are consistent. However, as with drifts and story shears, the simulations produce larger demands than recordings in the fault-normal direction as evidenced by SMRF column and beam demand-to-limit ratios. This increase can again be attributed to the heightened polarization of simulations and outliers in response. But despite the larger demands from simulations in the fault-normal direction, the two ground motion sets would generally
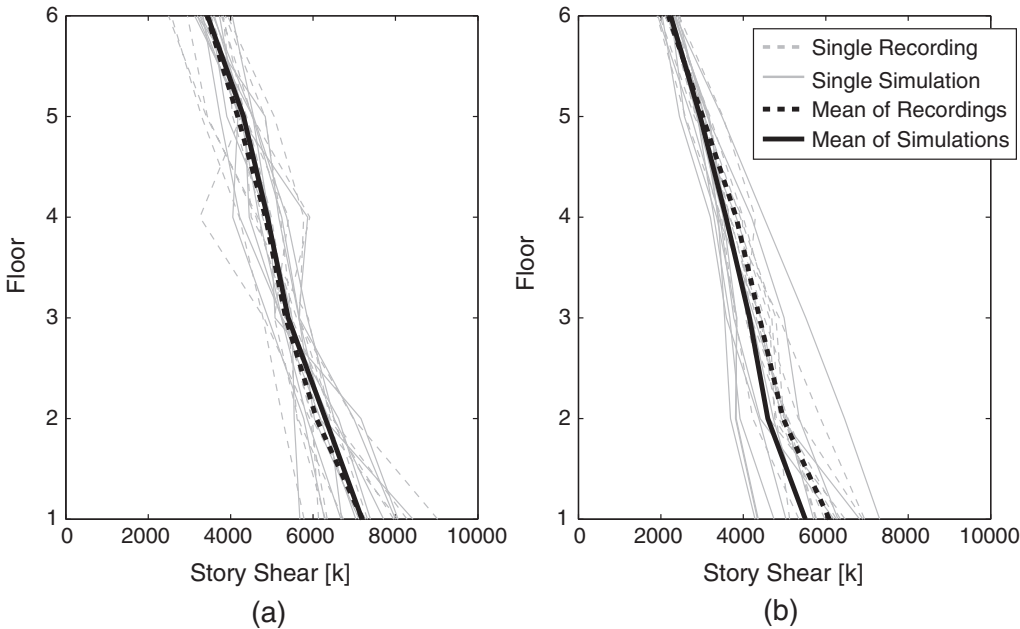

Figure 14. Story shear from the set of recorded and simulated ground motions in the (a) fault-normal and (b) fault-parallel directions.
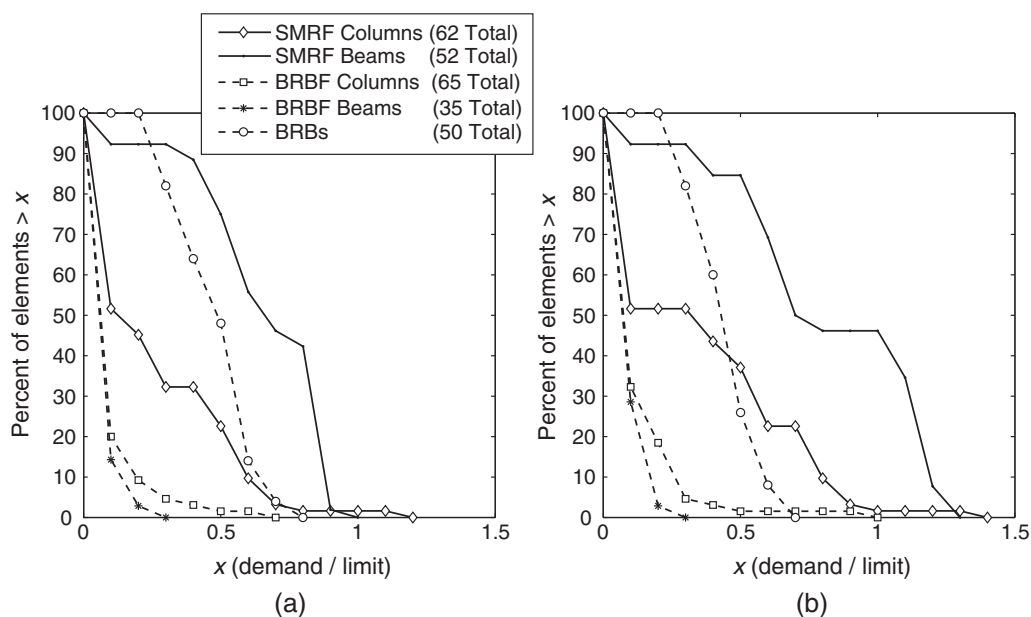
Figure 15. Mean component demand to limit ratio from nonlinear response history analysis using the ground motion (a) recordings and (b) simulations.

motivate similar design decisions, which is the ultimate goal of nonlinear response history analysis.

CONCLUSIONS

This study focused on the validation of hybrid broadband simulations for use by structural engineers as input to nonlinear response history analysis (as opposed to validation for seismic hazard analysis). The structural analysis procedure considered here was the proposed updated procedure for Chapter 16 of ASCE 7, though both the current ASCE 7-10 and the proposed update allow the use of "appropriate ground motion simulations". Both prefer ground motions from recordings but allow simulations if a sufficient number of recordings cannot be found, though they provide no instruction on their generation and selection.

We presented an example procedure for generating and selecting hybrid broadband simulations for a real building located in Berkeley, CA. First, we computed the target spectrum and selected a set of ground motion recordings following the proposed updated procedure in Chapter 16 of ASCE 7. Then, we used the SCEC Broadband Platform to generate 120 hybrid broadband simulations from the earthquake scenario controlling the seismic hazard at the building site and selected 11 simulations that best matched the recordings. Simulations were selected to match recordings because the goal of this study was to control for elastic spectral response and identify discrepancies in structural response due to other properties, though future studies may consider selecting recordings and simulations to match the target spectrum and check for other discrepancies, such as variability of the response spectra.

Finally, we evaluated the structural performance under the recordings and simulations using PERFORM-3D and found that the predicted performance was similar.

Although we were easily able to generate and select a set of simulations satisfying the code criteria, their directional properties differed somewhat from comparable recordings. The average ratio of fault-normal to fault-parallel response spectra of the simulations was up to 2.5 times larger than recordings at long periods. And the $Sa_{RotD100}$ to Sa_{RotD50} ratios were on average larger than expected, indicating that the amplitude of the simulations varies strongly with orientation and that the simulations will tend to polarize structural response more than recordings. While the differences may in small part be due to the inability of recordings to represent ground motions at very near-fault sites, it is believed that they are primarily due to simplifications of the hybrid broadband method on the broadband platform, such as the use of 1-D Green's functions, 1-D velocity models, and single planar faults.

Despite these differences in directional properties, the overall structural performance from the recordings and the simulations were comparable. Discrepancies in the structural response can be partially explained by the larger fault-normal amplitude of the simulations, but the global behavior and, more importantly, resulting design decisions were similar. This result indicates that the use of hybrid broadband simulations as input to nonlinear response history analysis can be valid in certain cases, especially when the simulations' response spectra match the target spectrum, given the empirical and intuitive knowledge that elastic response spectra are strongly predictive of the response of structures. Given this, it can be anticipated that these simulations and recordings may produce greater discrepancies in response in, for example, a more flexible structure that is sensitive to long-period excitation where the two sets of motions differed more greatly.

In conclusion, hybrid broadband simulations have at least two important applications in engineering: (1) seismic hazard analysis and (2) nonlinear response history analysis of structural models. Most validation efforts of hybrid broadband simulations have focused on the first application by investigating the reality of ground motion amplitudes such as shaking intensity and spectral acceleration for scenario earthquake events. This study focused on the second application because it reflects how most practicing engineers will interact with simulations. We selected hybrid broadband simulations and recordings with comparable spectra, both of which satisfied building code criteria, used them as input to a 3-D, real-world structural model designed by Rutherford + Chekene, and found that the structural performance and design decisions were similar in both cases.

REFERENCES

Aagaard, B. T., Brocher, T. M., Dolenc, D., Dreger, D., Graves, R. W., Harmsen, S., Hartzell, S., Larsen, S., and Zoback, M. L., 2008. Ground-motion modeling of the 1906 San Francisco earthquake, Part I: validation using the 1989 Loma Prieta earthquake, *Bulletin of the Seismological Society of America* **98**, 989–1011.

Aagaard, B. T., Graves, R. W., Rodgers, A., Brocher, T. M., Simpson, R. W., Dreger, D., Petersson, N. A., Larsen, S. C., Ma, S., and Jachens, R. C., 2010. Ground-motion modeling of Hayward Fault scenario earthquakes, Part II: simulation of long-period and broadband ground motions, *Bulletin of the Seismological Society of America* **100**, 2945–2977.

American Society of Civil Engineers/Structural Engineering Institute (ASCE), 2010. *Minimum design loads for buildings and other structures, ASCE 7-10*, Reston, VA.

Beresnev, I. A., and Atkinson, G. M., 1997. Modeling finite-fault radiation from the omega n spectrum, *Bulletin of the Seismological Society of America* **87**, 67–84.

Beyer, K., and Bommer, J. J., 2006. Relationships between median values and between aleatory variabilities for different definitions of the horizontal component of motion, *Bulletin of the Seismological Society of America* **96**, 1512–1522.

Boore, D. M., 1983. Stochastic simulation of high-frequency ground motions based on seismological models of the radiated spectra, *Bulletin of the Seismological Society of America* **73**, 1865–1894.

Boore, D. M., 2010. Orientation-independent, nongeometric-mean measures of seismic intensity from two horizontal components of motion, *Bulletin of the Seismological Society of America* **100**, 1830–1835.

Boore, D. M., Watson-Lamprey, J., and Abrahamson, N. A., 2006. Orientation-independent measures of ground motion, *Bulletin of the Seismological Society of America* **96**, 1502–1511.

Bray, J. D., and Rodriguez-Marek, A., 2004. Characterization of forward-directivity ground motions in the near-fault region, *Soil Dynamics and Earthquake Engineering* **24**, 815–828.

Building Seismic Safety Council (BSSC), 2009. *NEHRP Recommended Seismic Provisions for New Buildings and Other Structures, FEMA Report No. P-750*, National Institute of Building Sciences, Washington, D.C.

Burks, L. S., and Baker, J. W., 2014. Validation of ground motion simulations through simple proxies for the response of engineered systems, *Bulletin of the Seismological Society of America* **104**, 1930–1946.

Chiou, B., Darragh, R., Gregor, N., and Silva, W., 2008. NGA project strong-motion database, *Earthquake Spectra* **24**, 23–44.

Der Kiureghian, A., and Crempien, J., 1989. An evolutionary model for earthquake ground motion, *Structural Safety* **6**, 235–246.

Frankel, A., 2009. A constant stress-drop model for producing broadband synthetic seismograms: comparison with the Next Generation Attenuation Relations, *Bulletin of the Seismological Society of America* **99**, 664–680.

Galasso, C., Zareian, F., Iervolino, I., and Graves, R.W., 2012. Validation of Ground-Motion Simulations for Historical Events Using SDoF Systems. *Bulletin of the Seismological Society of America* **102**, 2727–2740.

Galasso, C., Zhong, P., Zareian, F., Iervolino, I., and Graves, R. W., 2013. Validation of ground-motion simulations for historical events using MDoF systems, *Earthquake Engineering & Structural Dynamics* **42**, 1395–1412.

Graves, R. W., and Pitarka, A., 2010. Broadband ground-motion simulation using a hybrid approach, *Bulletin of the Seismological Society of America* **100**, 2095–2123.

Hanks, T. C., and McGuire, R. K., 1981. The character of high-frequency strong ground motion, *Bulletin of the Seismological Society of America* **71**, 2071–2095.

Hartzell, S., Guatteri, M., Mai, P. M., Liu, P.-C., and Fisk, M., 2005. Calculation of broadband time histories of ground motion, part ii: kinematic and dynamic modeling using theoretical green's functions and comparison with the 1994 Northridge earthquake, *Bulletin of the Seismological Society of America* **95**, 614–645.

Hartzell, S., Harmsen, S., Frankel, A., and Larsen, S., 1999. Calculation of broadband time histories of ground motion: Comparison of methods and validation using strong-ground motion from the 1994 Northridge earthquake, *Bulletin of the Seismological Society of America* **89**, 1484–1504.

Haselton, C. B., Fry, A., Baker, J. W., Hamburger, R. O., Whittaker, A. S., Stewart, J. P., Elwood, K. J., Luco, N., Hooper, J. D., and Charney, F. A., 2014. Response history analysis for the design of new buildings: Part I - development of recommendations for the NEHRP provisions and the ASCE/SEI 7 standard, *Earthquake Spectra*, in review.

Iervolino, I., De Luca, F., and Cosenza, E., 2010. Spectral shape-based assessment of SDOF nonlinear response to real, adjusted and artificial accelerograms, *Engineering Structures* **32**, 2776–2792.

Jayaram, N., and Shome, N., 2012. A statistical analysis of the response of tall buildings to recorded and simulated ground motions, in *15th World Conference on Earthquake Engineering*, Lisbon, Portugal, 1–10.

Jones, P., and Zareian, F., 2013. Seismic response of a 40-story buckling-restrained braced frame designed for the Los Angeles region, *The Structural Design of Tall and Special Buildings* **22**, 291–299.

Jurkevics, A., and Ulrych, T. J., 1978. Representing and simulating strong ground motion, *Bulletin of the Seismological Society of America* **68**, 781–801.

Mai, P. M., Imperatori, W., and Olsen, K. B., 2010. Hybrid broadband ground-motion simulations: combining long-period deterministic synthetics with high-frequency multiple S-to-S backscattering, *Bulletin of the Seismological Society of America* **100**, 2124–2142.

Mobarakeh, A. A., Rofooei, F. R., and Ahmadi, G., 2002. Simulation of earthquake records using time-varying Arma (2,1) model, *Probabilistic Engineering Mechanics* **17**, 15–34.

Motazedian, D., and Atkinson, G. M., 2005. Stochastic finite-fault modeling based on a dynamic corner frequency, *Bulletin of the Seismological Society of America* **95**, 995–1010.

Pousse, G., Bonilla, L. F., Cotton, F., and Margerin, L., 2006. Nonstationary stochastic simulation of strong ground motion time histories including natural variability: application to the K-Net Japanese database, *Bulletin of the Seismological Society of America* **96**, 2103–2117.

Rezaeian, S., and Der Kiureghian, A., 2010. Simulation of synthetic ground motions for specified earthquake and site characteristics, *Earthquake Engineering & Structural Dynamics* **39**, 1155–1180.

Rutherford + Chekene, 2002. *Geotechnical Investigation Final Report for Units 1 and 2 Housing Project*, University of California, Berkeley.

Southern California Earthquake Center (SCEC), 2012. Broadband Platform (version 11.2.3), available at http://scec.usc.edu/scecpedia/Broadband_Platform.

Schmedes, J., Archuleta, R., and Lavallee, D., 2010. Correlation of earthquake source parameters inferred from dynamic rupture simulations, *Journal of Geophysical Research* **115**, B03304, doi:10.1029/2009JB006689.

Shahi, S. K., and Baker, J. W., 2011. An empirically calibrated framework for including the effects of near-fault directivity in probabilistic seismic hazard analysis, *Bulletin of the Seismological Society of America* **101**, 742–755.

Shahi, S. K., and Baker, J. W., 2013. *NGA-West2 Models for Ground-Motion Directionality, Pacific Earthquake Engineering Research Center Report 2013/10*, University of California, Berkeley.

Star, L. M., Stewart, J. P., and Graves, R. W., 2011. Comparison of ground motions from hybrid simulations to NGA prediction equations, *Earthquake Spectra* **27**, 331–350.

U.S. Geological Survey (USGS), 2008. 2008 Interactive Deaggregations (Beta), available at https://geohazards.usgs.gov/deaggint/2008/.

Wells, D. L., and Coppersmith, K. J., 1994. New empirical relationships among magnitude, rupture length, rupture width, rupture area, and surface displacement, *Bulletin of the Seismological Society of America* **84**, 974–1002.

Zeng, Y., Anderson, J. G., and Yu, G., 1994. A composite source model for computing realistic synthetic strong ground motions, *Geophysical Research Letters* **21**, 725–728.

Zimmerman, R. B., Baker, J. W., Haselton, C. B., Bono, S., Hooper, J., Engel, A., Hamburger, R., Celikbas, A., and Jalalian, A., 2014. Response history analysis for the design of new buildings: Part II - example applications to illustrate the recommended methodology, *Earthquake Spectra*, in review.